

JGR Solid Earth

RESEARCH ARTICLE

10.1029/2024JB029268

Key Points:

- Significant anisotropy is revealed in the Himalayan block, where previous studies suggest pervasively null measurements
- The crust significantly impacts observed anisotropy in teleseismic shear wave splitting, potentially leading to double-layered anisotropy
- Asthenospheric upwelling through a slab window beneath the Himalayan block accounts for the pervasive null measurements

Supporting Information:

Supporting Information may be found in the online version of this article.

Correspondence to:

K. H. Liu,
liukh@mst.edu

Citation:

Shen, C., Gao, S. S., Kong, F., & Liu, K. H. (2024). Tectonic implications of seismic anisotropy layering beneath the southern Tibetan plateau revealed by integrated shear wave splitting and receiver function analyses. *Journal of Geophysical Research: Solid Earth*, 129, e2024JB029268. <https://doi.org/10.1029/2024JB029268>

Received 7 APR 2024

Accepted 6 AUG 2024

Author Contributions:

Conceptualization: Stephen S. Gao, Kelly H. Liu

Data curation: Cong Shen

Formal analysis: Cong Shen

Funding acquisition: Kelly H. Liu

Investigation: Cong Shen

Methodology: Fansheng Kong, Kelly H. Liu

Project administration: Kelly H. Liu

Resources: Stephen S. Gao, Kelly H. Liu

Software: Stephen S. Gao, Fansheng Kong, Kelly H. Liu

Supervision: Stephen S. Gao, Kelly H. Liu

Validation: Fansheng Kong, Kelly H. Liu

Visualization: Cong Shen, Stephen S. Gao, Fansheng Kong

Writing – original draft: Cong Shen

Writing – review & editing: Cong Shen, Stephen S. Gao, Fansheng Kong, Kelly H. Liu

Writing – review & editing: Cong Shen, Stephen S. Gao, Fansheng Kong, Kelly H. Liu

Writing – review & editing: Cong Shen, Stephen S. Gao, Fansheng Kong, Kelly H. Liu

Writing – review & editing: Cong Shen, Stephen S. Gao, Fansheng Kong, Kelly H. Liu

Writing – review & editing: Cong Shen, Stephen S. Gao, Fansheng Kong, Kelly H. Liu

Writing – review & editing: Cong Shen, Stephen S. Gao, Fansheng Kong, Kelly H. Liu

Writing – review & editing: Cong Shen, Stephen S. Gao, Fansheng Kong, Kelly H. Liu

Writing – review & editing: Cong Shen, Stephen S. Gao, Fansheng Kong, Kelly H. Liu

Writing – review & editing: Cong Shen, Stephen S. Gao, Fansheng Kong, Kelly H. Liu

Writing – review & editing: Cong Shen, Stephen S. Gao, Fansheng Kong, Kelly H. Liu

Writing – review & editing: Cong Shen, Stephen S. Gao, Fansheng Kong, Kelly H. Liu

Writing – review & editing: Cong Shen, Stephen S. Gao, Fansheng Kong, Kelly H. Liu

Writing – review & editing: Cong Shen, Stephen S. Gao, Fansheng Kong, Kelly H. Liu

Writing – review & editing: Cong Shen, Stephen S. Gao, Fansheng Kong, Kelly H. Liu

Tectonic Implications of Seismic Anisotropy Layering Beneath the Southern Tibetan Plateau Revealed by Integrated Shear Wave Splitting and Receiver Function Analyses

Cong Shen¹ , Stephen S. Gao¹ , Fansheng Kong^{1,2} , and Kelly H. Liu¹ 

¹Department of Earth Sciences and Engineering, Missouri University of Science and Technology, Rolla, MO, USA, ²Key Laboratory of Submarine Geosciences, State Oceanic Administration & Second Institute of Oceanography, Ministry of Natural Resources, Hangzhou, China

Abstract To investigate continental dynamics underneath the south-central Tibetan plateau, which composes the Himalayan, Lhasa, and Qiangtang blocks, we have conducted comprehensive examinations of seismic azimuthal anisotropy in the crust using receiver functions (RFs) and crustal and mantle anisotropy using teleseismic shear wave splitting (SWS) analysis. In the Qiangtang block, the observed predominantly E-W fast orientations from RF and SWS analyses with similar magnitude are interpreted as resulting from eastward crustal flow with minor contributions from the mantle. In the Lhasa block, the crustal anisotropy is approximately N-S oriented, which is parallel to the strike of rift basins and southward crustal flow. Anisotropy revealed by SWS demonstrates a rotation from E-W in the north to NE-SW in the south, which can be interpreted as reflecting mantle flow field induced by the northward movement of the subducting Indian plate. The addition of PKS and SKKS measurements and extension of epicentral distance range to 171.8° for SWS analysis revealed dominantly strong E-W oriented anisotropy in most parts of the Himalayan block, where most previous studies reported pervasively null measurements. The absence of azimuthal anisotropy is observed in two regions in the Himalayan block which is attributable to mantle upwelling through a previously identified slab window. A two-layered anisotropy structure with different fast orientations for the upper and lower layers can be constrained in the southern Qiangtang and the vicinity of the Main Boundary Thrust.

Plain Language Summary In our study exploring the underground dynamics beneath the south-central Tibetan plateau, an area encompassing the Himalayan, Lhasa, and Qiangtang blocks, we utilized advanced seismic techniques to uncover the structure and dynamics of the earth's crust and mantle. In the Qiangtang region, our findings suggest an eastward crustal movement with minimal mantle influence. In the Lhasa block, the observed crustal anisotropy aligns with rift basins with a reduced magnitude, indicating a smaller-scale southward flow. In the same area, we also observed a transition in mantle flow patterns from east-west in the north to northeast-southwest in the south, attributed to the northward movement of the Indian plate. Contrary to previous studies that mostly found no anisotropy in the Himalayan block, our research detected strong anisotropy with east-west orientations. In two areas of the Himalayan block, the absence of anisotropy likely results from molten rock rising through a gap in the Indian plate. Moreover, we discovered a two-layered structure of rock alignment near the Main Boundary Thrust and the Qiangtang block.

1. Introduction

Numerous observational and laboratory studies have demonstrated that the lower crust and asthenosphere, representing mechanically weak zones relative to the more rigid overlying upper crust and lithospheric mantle, respectively, play a critical role in accommodating strain and the dynamical processes of driving plate movements (Jolivet et al., 2018; McKenzie, 1978; Molnar et al., 1993; Silver, 1996). These weak zones allow for the horizontal movement of tectonic plates and isostatic adjustments leading to vertical movements of lithospheric blocks (Hollister & Crawford, 1986). Such movements are mostly responsible for generating structural or lithological fabrics in the crust and upper mantle, which can in turn be used to reveal the existence and characteristics of past and ongoing tectonic events such as the continental convergence occurring along the Himalayas over the past 55 million years (Agius & Lebedev, 2017; Conrad & Behn, 2010; Jin et al., 1996; McKenzie, 1978).

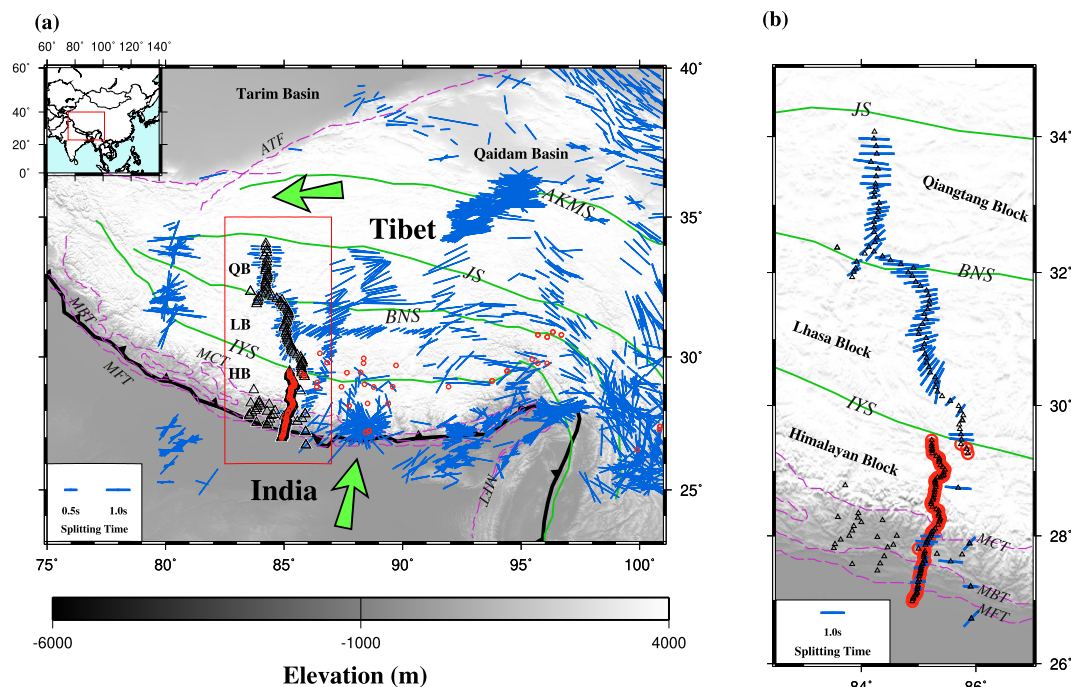


Figure 1. (a) Map showing major geophysical and geological features in the studying area (red rectangle) and adjacent regions. Blue bars indicate non-null SWS results, while red circles indicate locations of null measurements from previous studies (Chen et al., 2010, 2015; Sandvol et al., 1997; Singh et al., 2006). Black triangles are the stations used in this study. Green arrows denote the absolute plate motion direction of the Eurasian and Indian plates calculated by the HS3-NUVEL-1A plate model (Gripp & Gordon, 2002). MFT: Main Frontal Thrust; MBT: Main Boundary Thrust; MCT: Main Central Thrust; IYS: Indus-Yarlung suture; BNS: Bangong-Nujiang suture; JS: Jinshajiang suture; ATF: Altyn Tagh Fault; HB: Himalaya Block; LB: Lhasa Block; QB: Qiangtang Block. (b) Enlargement of the study area outlined by the red rectangle. Note that only the shear wave splitting measurements recorded by the stations used in this study are shown.

The Tibetan plateau, generally regarded as the consequence of a series of subductions and subsequent collisions of continental blocks, has been the focus of numerous studies aiming at understanding the complex tectonic processes involved in continental collision during the last several decades (e.g., Zhao et al., 1993; Zhou & Lei, 2016). The relative plate motion between the northward-moving Indian plate and the westward-moving Eurasian plate in the hotspot reference frame (Gripp & Gordon, 2002) is fundamentally responsible for the extensive changes in the topography, structure, and sedimentary facies of the plateau since the Late Cretaceous (Yin & Harrison, 2000). Before the collision, the pre-existing Tethys was extruded under the action of the northward thrust of the Indian plate, and its oceanic lithosphere descended underneath the Eurasian plate (Hsü et al., 1995). This and previous continental convergence have led to the amalgamation of the Himalayan, Lhasa, and Qiangtang blocks from south to north, bordered by the Indus-Yarlung, Bangong-Nujiang, and Jinshajiang sutures, respectively (Figure 1). In addition, the collision triggered numerous secondary structures (Molnar et al., 1973), including the N-S trending rifts (Nie et al., 2020), orogeny-parallel thrusts (Langille et al., 2010), and active detachments (Kapp et al., 2008). Exploring subsurface structure and dynamics in the crust and upper mantle is essential for understanding the formation mechanisms of the tectonic features observed on the plateau.

Seismic azimuthal anisotropy is widely utilized for probing crustal and upper mantle deformation and plastic flow (e.g., Chen et al., 2010; Hess, 1964; Silver & Chan, 1991; Wu et al., 2015; Zhang et al., 2023). In the upper mantle, the lattice-preferred orientation of anisotropic minerals, predominantly olivine, formed in response to simple shear associated with mantle flow, generates flow-parallel seismic anisotropy under normal mantle conditions (Ismail & Mainprice, 1998). Anisotropy could also be induced by past tectonic processes, which were then frozen into the rigid lithosphere (Silver, 1996). In the lower crust, amphibole and mica are highly anisotropic minerals that can lead to non-negligible anisotropy compared to the upper mantle, with a resulting orientation consistent with the simple shear direction (Christensen, 1984; Ko & Jung, 2015). In contrast, anisotropy in the upper crust is

mainly associated with the alignment of fluid-filled cracks (Crampin, 1981), with a resulting orientation parallel to the maximum compression direction.

Numerous studies on seismic anisotropy have been conducted in the south-central Tibetan plateau to investigate geodynamic processes associated with continental collision (e.g., Chen et al., 2010; Fu et al., 2008; Gilligan & Priestley, 2018; Hirn et al., 1995). Chen et al. (2010) analyzed 51 SKS and SKKS events recorded by 86 stations in the Hi-CLIMB array. They observed a strong E-W-oriented anisotropy in the southern Qiangtang block and the northern Lhasa block, and NE-SW-oriented anisotropy in the southern Lhasa block (Figure 1). An abrupt northward increase in seismic anisotropy at $\sim 33^{\circ}\text{N}$ in the Qiangtang block was inferred to mark the subducted Indian slab front (Chen et al., 2010, 2015; Sandvol et al., 1997; Singh et al., 2006). The pattern of anisotropy exhibits a clockwise rotation from E-W in the north near the Bangong-Nujiang suture to N-S in the south near the Indus-Yarlung suture (Chen et al., 2010), challenging earlier interpretations of isotropic Indian lithosphere front (e.g., Sandvol et al., 1997; Singh et al., 2006). Such a rotational pattern is attributed to the presence of crustal channel flow (Basuyau et al., 2013; Gilligan & Priestley, 2018; Lease et al., 2012). In the Himalayan block, pervasive weak anisotropy measurements were observed by over 90% of the Hi-CLIMB and portable stations (e.g., Chen et al., 2010; Chen & Özalaybey, 1998; Fu et al., 2008), with the formation mechanism still under debate. Distinct geodynamic models proposed either a localized mantle upwelling (Fu et al., 2008) or an isotropic Indian lithosphere (e.g., Chen & Özalaybey, 1998) as explanations.

Investigations of seismic velocity heterogeneity beneath the southern and central Tibetan plateau suggested that the Indian slab is torn into several segments, each characterized by different dipping angles and sizes (Chen et al., 2015; Duan et al., 2017), with three lithosphere breakage bands distinguished by low Pn and S-velocity zones (Jiang et al., 2014; Li & Song, 2018). Increasing evidence suggests that crustal anisotropy on the Tibetan plateau could contribute significantly (up to 50%) to the observed anisotropy measurements using splitting of the PKS, SKKS, and SKS phases (Agius & Lebedev, 2017; Wu et al., 2015). While the structural frameworks within the crust and upper mantle of the central Tibetan plateau are well established, the deformation fields in the crust and upper mantle and their formation mechanisms remain poorly understood and controversial (e.g., Chen et al., 2010; Fu et al., 2008). These controversies are likely related to the inherent limitations of the approaches used, notably shear wave splitting (SWS) analyses, which provide high horizontal but lack vertical resolution (e.g., Long & Silver, 2009; Savage, 1999). This limitation impedes our understanding of deformation fields. Thus, additional investigations on anisotropy depth and layered structures are necessary to isolate crustal contribution and better constrain upper mantle anisotropy. In particular, confirming or rejecting the previously observed dominantly null measurements in the Himalayan block and proposing a viable mechanism for the observed anisotropy is essential for understanding mantle dynamics in the archetypical continental collision zone.

In this study, we have incorporated additional constraints on the deformation models by conducting a joint analysis of individual SWS parameters and receiver function-based crustal anisotropy measurements. Our goal is to explore the anisotropic structure present within the crust, lithospheric mantle, and asthenosphere, respectively. By increasing the coverage of back azimuth (BAZ) relative to previous SWS studies, through an expanded epicentral distance range and the inclusion of the PKS phase, the resulting anisotropy measurements demonstrate significant spatially varying anisotropy within both the crust and upper mantle, with deformations concentrated in the two mechanically weak layers, that is, the middle/lower crust and asthenosphere. In the Himalayan block, strong E-W oriented anisotropy is observed and is attributed mainly to sub-slab collision-zone parallel flow.

2. Data and Methods

Data used to obtain the SWS measurements were recorded by 141 broadband seismic stations, among which 120 were part of the 2002–2005 Hi-CLIMB array and 21 were from other portable experiments. All the data were obtained from the Seismological Facility for the Advancement of Geoscience Data Management Center. When a seismic shear wave goes through an anisotropic media, it tends to split into two waves, leading to an arrival time difference between the fast and slow wave components. In this study, we utilize source-normalized P-to-s conversions from the Moho (receiver functions or RFs) and teleseismic SWS analyses to compute the optimal splitting parameters (fast polarization orientation ϕ and delay time δt).

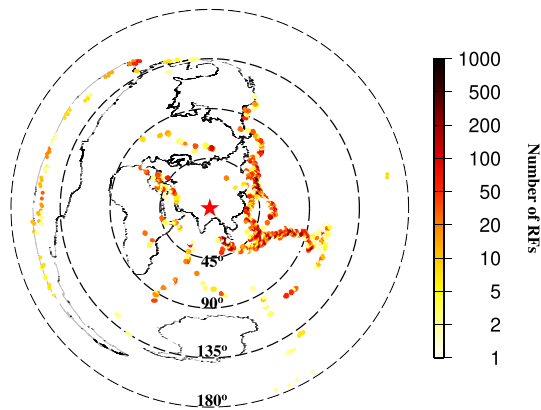


Figure 2. Azimuthal equidistant projection map showing the number of P-to-s receiver functions within circles of 1° radius used for crustal anisotropy analysis. The red star indicates the center of the Hi-CLIMB seismic network.

2.1. Measurements of Crustal Anisotropy Using Receiver Function Analysis

The seismograms used for receiver function analysis are from events with a cutoff magnitude of 4.5 and epicentral distances between 30.0° and 180° (Figure 2) and are band-pass filtered within the frequency range of 0.08–0.8 Hz. The RFs are then rotated to the RTZ (radial-transverse-vertical) coordinate system and are computed using a time-domain iterative deconvolution method (Ligorria & Ammon, 1999). Low-quality RFs are rejected following the signal-to-noise ratio selection criteria (Liu & Gao, 2013) to ensure data quality. A total of 21,901 radial RFs are selected from 1695 events (Figure 2) to investigate the crustal anisotropy.

We use the same procedure utilized by Kong et al. (2016) and Zheng et al. (2024) to quantify the bulk crustal anisotropy. After correcting the P-to-s conversion time ($P_{m,s}$) differences due to epicentral and focal depth differences (Zheng et al., 2018), the receiver functions are stacked using a grid-search method (Nair et al., 2006; Zhu & Kanamori, 2000) to estimate the

crustal thickness (H) and V_p/V_s (κ), which are subsequently used as a constraint for picking the $P_{m,s}$ phase. Examples of crustal anisotropy measurements for Stations H1020 and H1540 can be found in Figures S1 and S2 in Supporting Information S1.

Under the assumption of a single layer of anisotropy with a horizontal axis of symmetry, the moveout of the converted phases from the Moho ($P_{m,s}$) satisfies the sinusoidal function in terms of the BAZ (Kong et al., 2016; Rümpker et al., 2014). Since the $P_{m,s}$ phase arrival time repeats every 180°, we adjust stations with BAZs over 180° by subtracting 180°, grouping them into the 0–180° range to determine the anisotropy parameters for these stations. All the RFs are grouped into consecutive 10° azimuthal bins based on their BAZ. Anisotropy parameters are derived from the grouped RFs through curve fitting of the $P_{m,s}$ arrival times corresponding to the maximum amplitudes using a nonlinear least-squares algorithm as well as through grid search to identify optimal parameters for maximum stacking amplitude (Wu et al., 2015).

Considering the wide range of Moho depths in the study area (Nabelek et al., 2009), we employ a search range of 0.0–2.0 s for δt with an increment of 0.1 s and a \varnothing range of -90° – 90° with a 1° increment. The arithmetic means of δt and the angular mean of \varnothing are selected if the delay time difference from the two methods (i.e., curve-fitting and grid-searching) is less than 0.15 s, and the difference between two fast polarization orientations is less than 20°. For larger discrepancies in delay times and fast orientations between results from the two methods, the curve-fitting results are preferred for their stability compared to the grid-searching results. To ensure the robustness of the results, we manually verified the results to reject those with poor BAZ coverage and ambiguous $P_{m,s}$ arrival times. This step also involved adjusting the time window to exclude arrivals that are inconsistent with the calculated arrival time based on the crustal thickness derived from H- κ stacking.

2.2. Measurements of Seismic Anisotropy Using Shear Wave Splitting

The computation of the optimal splitting parameters from PKS, SKS, and SKKS (collectively known as XKS) is based on the transverse energy minimization method (Silver & Chan, 1991). The selected events for the SWS analysis have magnitudes (M_w) greater than 5.5 and epicentral distances between 84° and 180°. These events were band-pass filtered within the frequency range of 0.04–0.5 Hz. Events with a signal-to-noise ratio (SNR) less than 4.0 were discarded (Liu & Gao, 2013), resulting in 1348 qualifying events (Figure 3). Individual SWS parameters are manually checked and ranked following the procedure described in Liu and Gao (2013). A total of 851 high-quality individual splitting parameters are obtained for further analyses (Figure 4). Note that at some stations, while SKS and SKKS result in null measurements (Figures S3a and S3b in Supporting Information S1), the inclusion of the PKS phase which is mostly from the north (Figure 3c), leads to well-defined measurements (Figure S3c in Supporting Information S1).

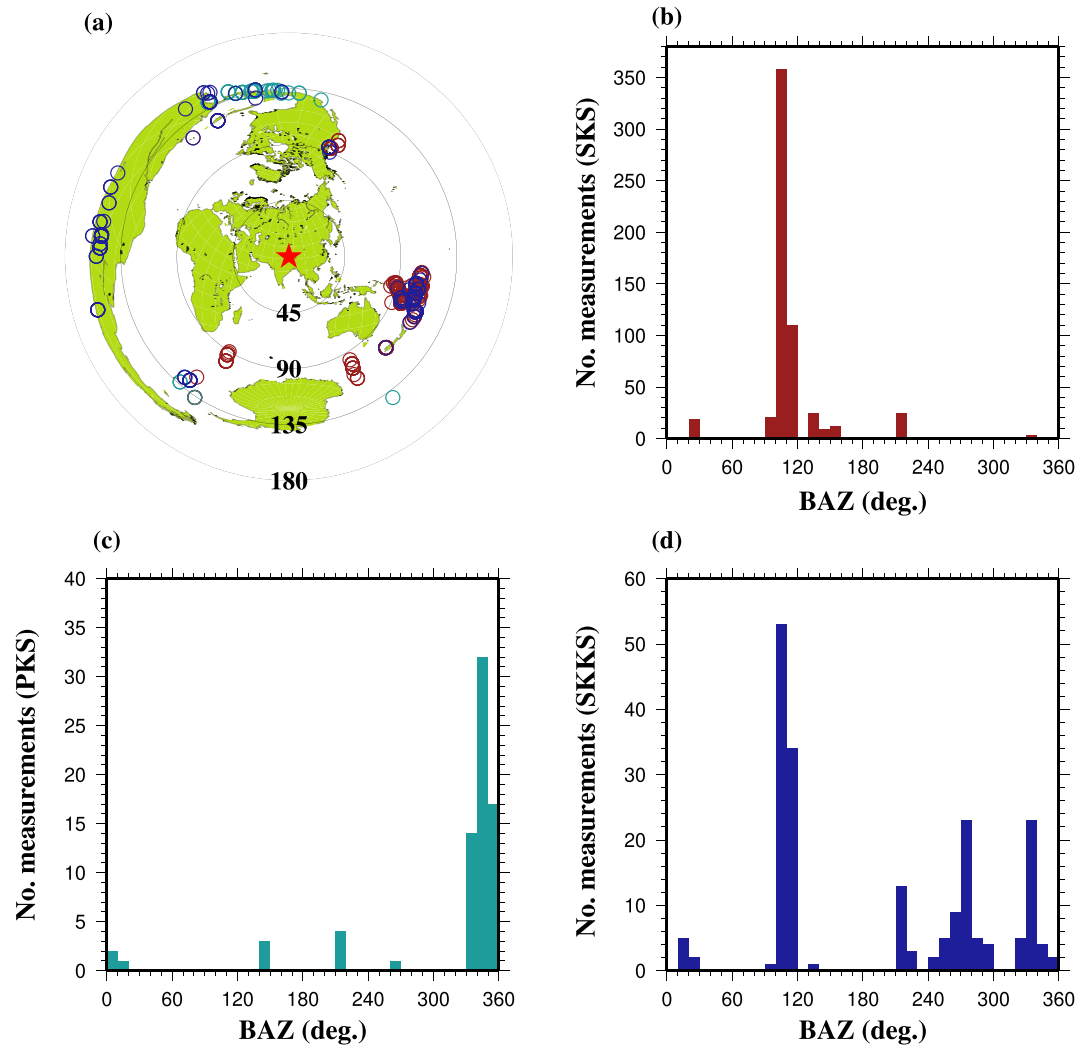


Figure 3. (a) Azimuthal equidistant map showing the distribution of earthquakes that resulted in well-constrained XKS splitting measurements. Events of the SKS, PKS, and SKKS are shown in mahogany, azure, and blue, respectively. The red star indicates the center of the study area. (b) Histogram showing the number of SKS phases and their back-azimuth distribution. (c) Similar to (b) but for PKS phases. (d) Similar to (b, c), but for SKKS phases.

2.3. Estimation of Anisotropy Depth

The XKS splitting parameters have excellent horizontal resolution due to the near-vertical incidence angle, however, the vertical resolution is relatively poor (Liu & Gao, 2011). To assess the anisotropy depth accounting for the XKS splitting measurements, the variation factor (F_v) is calculated with the optimal depth corresponding to the minimum variation factor (Liu & Gao, 2011). The study area is divided into three sub-blocks based on the characteristics of the observed splitting parameters (Figure 4a). For each sub-block, the individual splitting measurements are grouped into a series of circular bins with a radius of 0.2° , and a spacing distance of 0.2° . We calculate the standard deviation (SD) for each circle and then average them to obtain the SD value for a candidate anisotropy depth ranging from 0 to 250 km, with a step increment of 50 km (Figures S4, S5, and S6 in Supporting Information S1).

2.4. Characterization of Multilayer Anisotropy

The individual SWS measurements are systematically analyzed to distinguish between simple and complex anisotropy at each station. A 90° periodicity observed in terms of fast orientation and splitting time against the BAZs serves as a robust indicator of multi-layered anisotropic structures near the observation location (Gao &

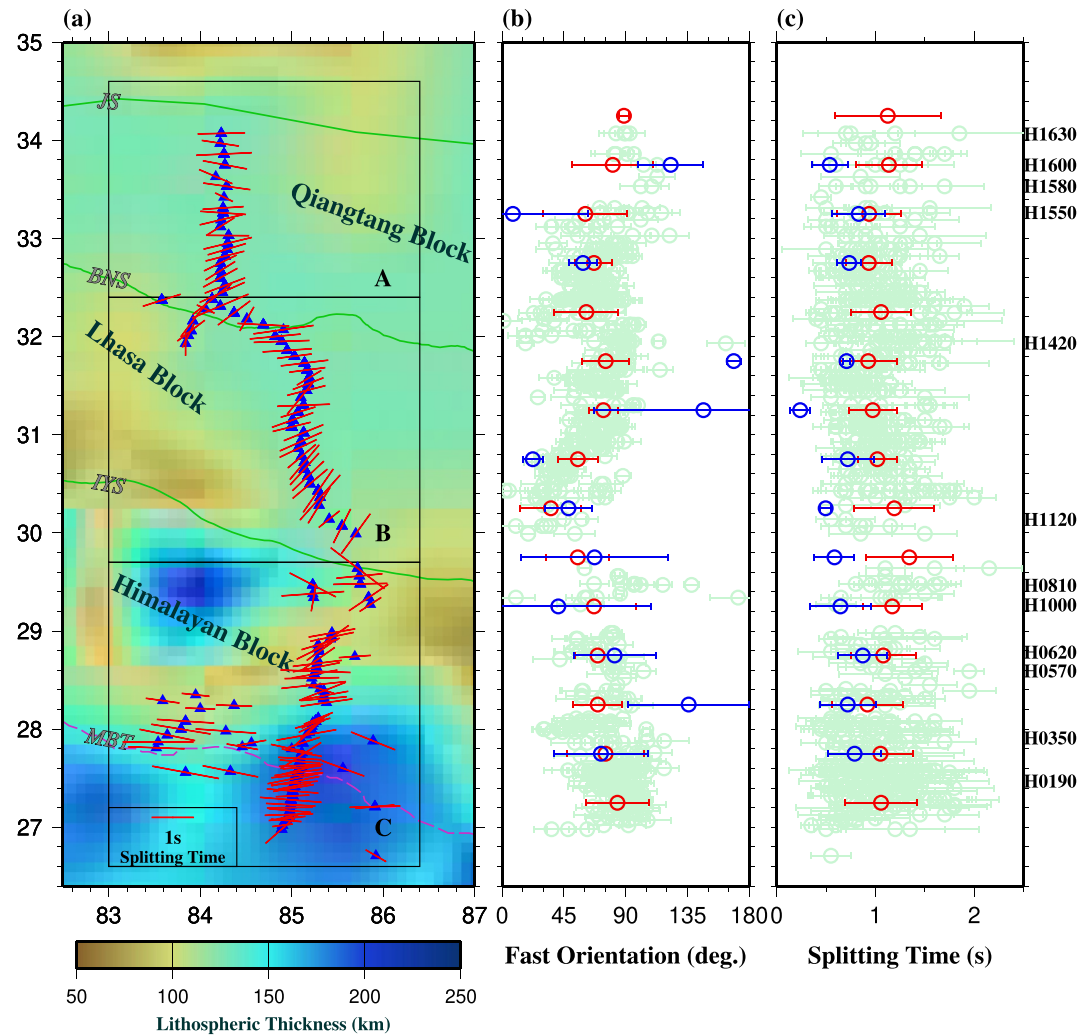


Figure 4. (a) Resulting station-averaged XKS splitting parameters (red bars) centered at the stations (blue triangles). (b) The distribution of fast orientations plotted against latitude. Red bars with circles indicate the averaged SWS parameters within 0.5° latitudinal ranges, while the blue bars represent averaged crustal anisotropy measurements within 0.5° latitudinal ranges. The light green bars represent the individual SWS results. (c) Similar to (b) but for splitting time.

Liu, 2009; Rumpker & Silver, 1998; Silver & Savage, 1994), while a 180° periodicity implies dipping anisotropic structure (Frederiksen & Bostock, 2000). Conversely, single-layer anisotropy or multilayer with identical or orthogonal fast orientations presents invariant splitting parameters with azimuth. Additionally, the anisotropy may be influenced by the piercing point if events recorded by the same station sample areas with different anisotropic features (Jia et al., 2021). To enhance the azimuthal coverage, we combine measurements from nearby stations displaying similar azimuthal variation patterns. For instance, as detailed in the next section, measurements from Stations H1490, H1500, H1510, H1520, H1530, and H1540 are combined to characterize complex anisotropy. Note that for simplicity, the combined data set is named H1500. For stations with sufficient azimuthal coverage, a grid-search algorithm is employed to calculate the splitting parameters from individual layers under a two-layer model (Gao & Liu, 2009; Silver & Savage, 1994).

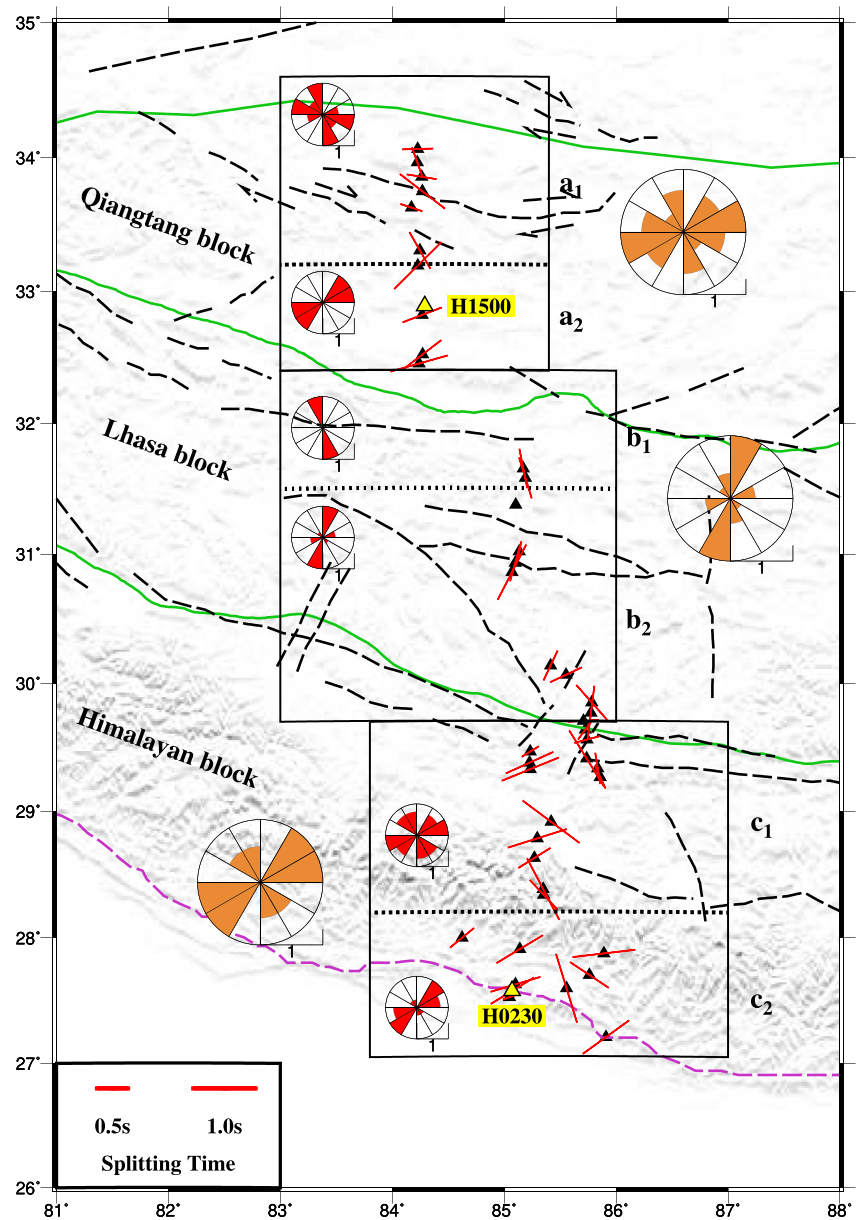


Figure 5. Resulting crustal anisotropy measurements (red bars). The rose diagrams within the blocks are the results of the sub-blocks separated by the dashed lines, whereas the ones outside the blocks show the results of the blocks delineated by the solid rectangles. The two high-lighted yellow triangles mark the locations of Stations H0230 and H1500 where two-layered anisotropy is investigated (Figure 6).

3. Results

3.1. Results of Crustal Anisotropy

A total of 43 stations (out of a total of 164 with at least one RF) have yielded reliable measurements for the interpretation of crustal anisotropy (Figure 5). The azimuthal variation of the $P_{m,s}$ arrivals is characterized by a periodicity of 180° , and the absence of other prominent periodicities suggests that crustal anisotropy in the study area is dominated by a horizontal axis of symmetry (Levin & Park, 1998). The delay time for the study area ranges from 0.15 to 1.18 s, with an average of 0.70 ± 0.28 s, which requires an anisotropy of 2%–9% assuming a crustal thickness of 65 km and a V_s of 4.5 km/s. The average delay time for the crust in our region is larger than that obtained in the studies conducted in northern and southeastern Tibet (Wu et al., 2019; Zheng et al., 2018), reflecting the significant role that the crust plays in seismic anisotropy in these areas. NE-SW fast orientations

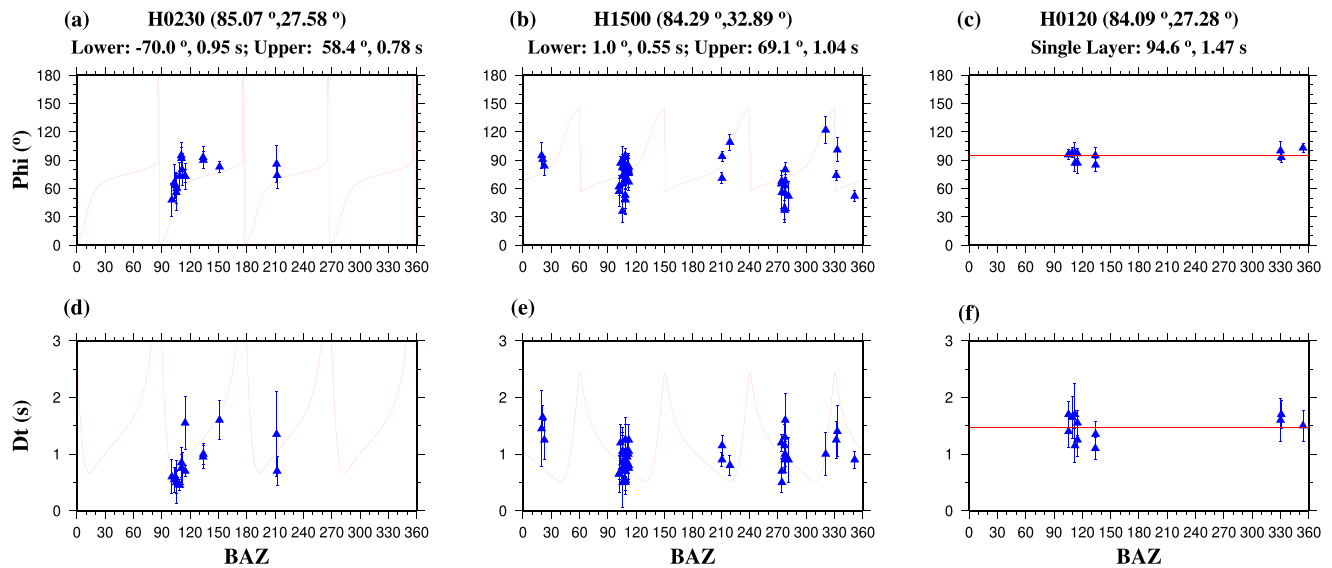


Figure 6. XKS splitting measurements exhibiting a periodicity of 90° in back-azimuthal (BAZ) or the character of a single layer. (a) Fast orientations for Station H0230. (d) Variation in splitting time for Station H0230. (b, e) similar to (a, d), respectively, but for Station H1500 and its adjacent stations. (c, f) similar to (a, d), but for Station H0120. Red lines illustrate the theoretical XKS distributions calculated by using the optimal splitting parameters of the upper and lower layers or single layer shown above.

dominate the northern and southern Himalayan block while some NW-SE fast orientations are sporadically observed at stations in the central and northeast parts of the block. Nearly N-S-oriented crustal anisotropy is observed in the Lhasa block. The northern Qiangtang block is characterized by mostly NW-SE oriented crustal anisotropy, while the southern Qiangtang block has NE-SW oriented anisotropy.

3.2. Results of XKS Splitting Measurements

A total of 851 high-quality individual SWS measurements from 141 stations, including 583 SKS, 194 SKKS, and 74 PKS, are obtained (Figures 3 and 4). To investigate spatially variable anisotropy origin, we divide the study area into three sub-blocks bounded by the sutures (Figure 4a). Unlike the previous studies (e.g., Chen et al., 2010; Fu et al., 2008; Huang et al., 2000) which reported dominant null or weak splitting measurements, we find significant seismic anisotropy south of the Indus-Yarlung suture (Area C in Figure 4a), with an average delay time of 1.05 ± 0.03 s. The fast orientations are E-W or NE-SW in the west of Area C, which is parallel to the mountain belt, rotate to SW-NE in the east near the Main Boundary Thrust, and return to E-W in the central part of this area. To the north of the Indus-Yarlung suture within the Lhasa block, the fast orientations show successive changes from NE-SW to W-E from the south to north, except for several measurements near 84.2°E , which are consistent with previous SWS studies (e.g., Chen et al., 2010). The largest delay time for a single measurement reaches 2.15 ± 0.33 s near the Indus-Yarlung suture. The averaged fast orientation and delay time are $60.05 \pm 23.41^\circ$ and 0.99 ± 0.04 s, respectively, in the Lhasa block. The fast orientations in the Qiangtang block are around E-W, with an average of $82.29 \pm 17.26^\circ$ for fast orientation and 0.98 ± 0.04 s for delay time.

Systematic investigation of the individual measurements indicates that most stations exhibit uniform splitting parameter distributions concerning the BAZ, indicating a single anisotropic layer with a horizontal axis of symmetry is sufficient to describe the major anisotropy characteristics. However, the two areas near the Himalayan thrust system and the Bangong-Nujiang suture exhibit a periodicity of 90° in both fast orientations and delay times (Figure 6).

3.3. Multilayer Anisotropy in the Himalayan and Qiangtang Blocks

Optimal splitting parameters for two anisotropic layers are determined through a grid-search approach, involving all possible parameter pairs within specified ranges (Gao & Liu, 2009; Silver & Savage, 1994). To mitigate non-uniqueness, we incorporate additional constraints by fixing the splitting parameters for the upper layer using the results obtained from the crustal anisotropy. For Station H0230, the values obtained for the lower layer (-69.0° ,

0.60 s) and the upper layer (77.0°, 0.65 s), without any constraints using the results from crust anisotropy in the Himalayan block (Station H0230, Figures S7a and S7c in Supporting Information S1), are consistent with those derived under the assumption that the anisotropy of upper layer originates from the crust (Figure 6a). However, significant differences in the resulting two-layer parameters are found for Station H1500. Without constraining the upper layer, the splitting parameters are (40.0°, 1.10 s) for the lower layer and (−70.0°, 0.60 s) for the upper layer (Figures S7b and S7d in Supporting Information S1), while by fixing the fast orientations of the upper layer to the parameters obtained from the crust, the resulting values become (−1.0°, 0.60 s) for the lower layer and (69.1°, 1.10 s) for the upper layer (Figures S7e and S7g in Supporting Information S1). This discrepancy is most likely related to the well-known non-uniqueness of the grid-searching process (Silver & Savage, 1994). To reduce the non-uniqueness, by considering the extremely strong crustal anisotropy with a delay time of 1.04 s in the area, we place a constraint of a larger delay time for the upper layer compared to that of the lower layer. The resulting splitting parameters are (25.0°, 0.65 s) for the lower layer and (81.0°, 0.70 s) for the upper layer (Figures S7f and S7h in Supporting Information S1), which are similar to the results when the upper layer is assumed to be the crust (Figures 6b and 6c). Across all models tested, the fast polarization orientation of the upper layer predominantly aligns with the east-west direction, while that of the lower layer aligns with the north-south direction.

3.4. Optimal Depth of the Observed Anisotropy

The optimal anisotropy depth in the Qiangtang block ranges from a few km to 50 km (Figure S4 in Supporting Information S1), suggesting that crustal and upper-most mantle anisotropy is responsible for the observed splitting measurements in the block. Conversely, in the Lhasa block, the minimum SD is located at a depth of approximately 150 km (Figure S5 in Supporting Information S1), slightly deeper than the lithospheric thickness of approximately 130 km (Pasyanos et al., 2014), implying that the primary source of anisotropy is probably located at the lithosphere-asthenosphere transitional zone. The anisotropy depth estimated for the Himalayan block is approximately 200 km (Figure S6 in Supporting Information S1), indicating that the anisotropy is present in the upper asthenosphere, given that the thickness of the lithosphere in this block ranges from 150 to 190 km (Pasyanos et al., 2014).

4. Discussion

SWS analyses across south central Tibet reveal substantial regional variations in anisotropy, highlighting a trend where anisotropic depths decrease from south to north. Specifically, anisotropy in the Himalaya block is predominantly located within the asthenosphere, while in the Lhasa block, it is situated at the lithosphere-asthenosphere transition zone, and in the Qiangtang block, it is primarily within the crust. Further investigations using P-to-s converted waves from the Moho indicate discrepancies between the crustal anisotropy and those derived from SWS, suggesting the presence of double-layer anisotropy. This hypothesis has been substantiated in both the Himalaya and Qiangtang blocks. Notably, the contribution of the crustal channel flow to the integrated crustal anisotropy in the Lhasa and Qiangtang blocks is different due to different flow directions and intensities.

4.1. Significant Crustal Flow in the Qiangtang Block

In the Qiangtang block, the dominant fast orientation of crustal anisotropy is E-W (Figure 5), which is consistent with the proposed direction of mid-to-lower crustal channel flow (Agius & Lebedev, 2017; Klempner, 2006; Li et al., 2022; Tao et al., 2022). An independent piece of evidence of strong crustal anisotropy comes from the resulting 0–50 km for the optimal depth estimation using XKS splitting measurements (Figure S4 in Supporting Information S1). Results from two-layer fitting for the combined data set in the southern part of the Qiangtang block (Figure 6b) also suggest that the crust is strongly anisotropic with a nearly E-W fast orientation. The splitting times range from 0.35 to 1.04 s, suggesting an anisotropy magnitude from 4% to 9% for a 50 km thick middle and lower crust. This is in agreement with previous crustal anisotropy studies in the Tibetan plateau. For instance, Wu et al. (2015) reported the delay time of the mid-to-lower crust beneath the western Tibet plateau ranges from 0.45 to 1.30 s, requiring an anisotropy of 5%–15%. Agius and Lebedev (2017) measured crustal anisotropy at multi-station experiments in the central Tibetan plateau and revealed E-W fast orientations and splitting times ranging from 0.25 to 0.80 s. They explained the observations as the alignment of the mica crystals driven by horizontal flow. Zhang et al. (2023) measured anisotropy at some of the stations that we used in this study and obtained similar E-W-orientated crustal anisotropy with a delay time of around 1.0 s near the Bangong-

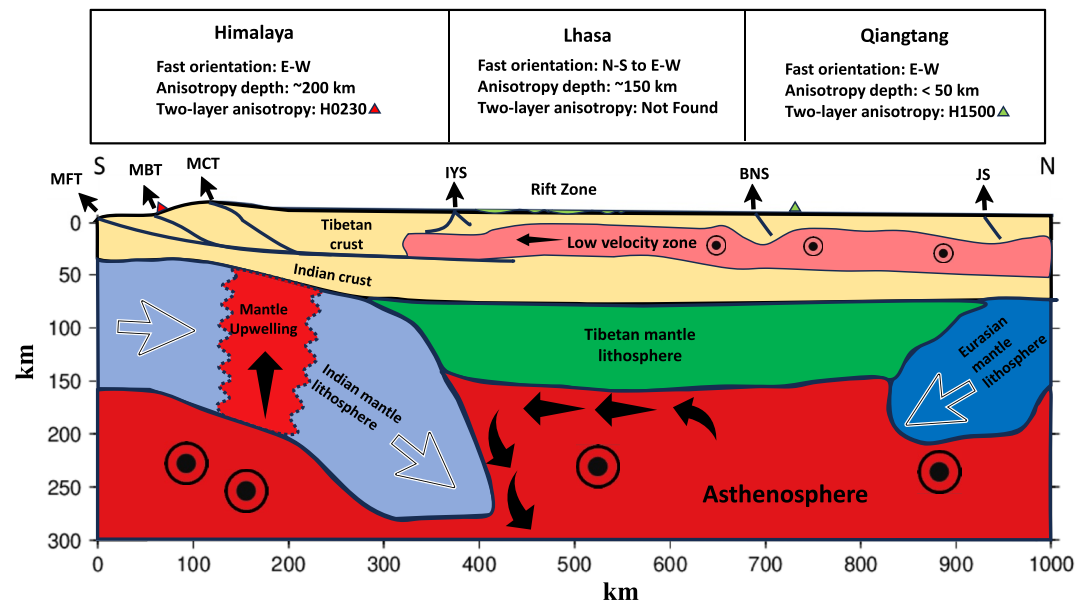


Figure 7. (top) Summary of major features in the observations. (bottom) Model illustrating the structure and driving mechanisms behind the observed anisotropy in the southern Tibetan plateau (modified from Wang et al., 2016). The E-W fast polarization orientations at the southern end of the study area result from asthenosphere flow. Slab breakage facilitates the upwelling of asthenospheric material. The mantle anisotropy in the Lhasa block, delineated by the Indus-Yarlung suture and the Bangong-Nujiang suture is induced by corner convective flow and the eastward movement of the mantle, while crust anisotropy is controlled by rifts and southward crustal flow. The dominant E-W anisotropy in the Qiangtang block characterizes the eastward mid to lower crust flow.

Nujiang suture. Our measurements using integrated receiver function and XKS splitting analyses provide additional evidence for eastward crustal flow in the Qiangtang block (Figure 7). By contrast, the lower layer of anisotropy at Station H1500 is characterized by a nearly N-S direction (Figure 7) and a smaller splitting time of 0.55 s. One of the possible explanations for the lower layer anisotropy is the southward subduction of the Eurasian mantle lithosphere beneath the Qiangtang block, as shown in Figure 7.

4.2. Potential Mid-Lower Crustal Flow in the Lhasa Block

Our crustal anisotropy measurements reveal that the fast orientations in the Lhasa block are sub-parallel to N-S trending rifts (Figure 5), which are commonly found in the Lhasa block and are generally considered to be the result of N-S compression (Yin & Harrison, 2000). Numerous previous studies have demonstrated that extensional fractures in the top several kilometers of the upper crust formed in compression domains can produce anisotropy with a fast orientation that is parallel to the direction of the compressional stress (Crampin, 1981). In areas with a normal crustal thickness, the splitting times are normally smaller than 0.1 s (e.g., Shi et al., 2013), while in areas with thickened crust such as the eastern Tibetan plateau, it could amount to 0.2 s (e.g., Hu et al., 2019). This is significantly smaller than the splitting times that we observed in the Lhasa block, which range from 0.30 to 0.97 s (Figure 5). Therefore, other mechanisms besides stress-induced anisotropy must have contributed to the observed crustal anisotropy.

Previous studies using ambient noise (e.g., Guo et al., 2009) and body wave tomography (e.g., Hung et al., 2010) have identified a pronounced low-velocity zone in the mid-to-lower crust beneath the Lhasa block, indicating a mechanically weak middle to lower crust (Hung et al., 2010; Jiang et al., 2014; Pang et al., 2018). One possible mechanism is southward mid-to-lower crustal flow that has been proposed by some studies based on isotopic observations and seismic velocity profile (Figure 7; Klemperer, 2006). Assuming that the extensional fractures in the upper crust contribute to 0.2 s of the observed crustal anisotropy, the mid-to-lower crustal flow accounts for about 0.5 s of the crustal splitting time. This is significantly smaller than that inferred for the mid-to-lower crustal flow underneath the Qiangtang block and may suggest a weaker channel flow in the former area. This may explain

the diverse perspectives among studies concerning the existence and direction of the channel flow in the Lhasa block among previous studies (Beaumont et al., 2004; Kapp et al., 2005).

4.3. Mantle Flow Fields Beneath the Lhasa Block

The fast orientations observed from XKS splitting in the Lhasa block show a systematic and gradual variation, from NE-SW in the southern portion of the block to E-W in the northern block. The splitting times from XKS splitting analysis are about twice of those from crustal anisotropy analysis at most of the stations in the area, suggesting a strong mantle contribution. Depth estimations of anisotropy within the Lhasa block indicate that its primary source is the lithosphere-asthenosphere transition zone. The fast orientations observed in the southern part of the Lhasa block are sub-parallel to the direction of the plate motion of the Indian plate (Figure 1). Numerous studies have shown that a subducting slab can induce a corner flow which in turn leads to fast orientations that are parallel to the direction of subduction (e.g., Fu et al., 2008; Lei et al., 2019). Therefore, the NE-SW fast orientations in the southern Lhasa block could be attributed to corner flow associated with the subduction of the Indian slab (Figure 7). The existence of NE-SW-oriented anisotropy in the southern Lhasa block can provide independent evidence for the presence of a mantle wedge, which is one of the debated issues on Tibetan mantle tomography (Hung et al., 2010; Zhang et al., 2016).

Progressing northward, the transition to an E-W anisotropy orientation could be interpreted as a result of the blockage of dispatched mantle flow associated with the advancing Indian slab by the thick lithosphere in the middle and northern parts of the Lhasa block (Figures 4a and 7). This model suggests that the direction of the movement of the asthenospheric material is in general agreement with that of the surface material. The flow fields proposed here to explain our XKS splitting results are similar to what is proposed by some other studies. For instance, a shift from N-S to E-W in the fast polarization orientation over brief spans has been identified in the eastern Tibetan plateau (Lei et al., 2019), which was explained as the consequence of material extrusion flow and orthogonal mantle convection within the big mantle wedge model.

4.4. Orogen-Parallel Mantle Flow in the Sub-Slab Region Beneath the Himalayan Block

In the Himalayan block, where most previous studies suggest a lack of observable azimuthal anisotropy (e.g., Chen et al., 2010; Fu et al., 2008), the fast orientations from XKS splitting are mostly E-W which are sub-parallel to the strike of the orogenic belt (Figure 4a). In addition, a nearly E-W lower layer anisotropy is revealed at Station H0230 (Figure 6a). Furthermore, the observed crustal anisotropy has spatially variable fast orientations and significantly smaller splitting times, and the estimated depth of anisotropy in this area is about 200 km, which is comparable to or deeper than the estimated lithospheric thickness (Figure 4a; Pasyanos et al., 2014). These observations suggest that the observed anisotropy is mostly from the upper asthenosphere. A viable mechanism for trench parallel anisotropy in typical subduction zones is sub-slab trench parallel flow, most likely driven by slab rollback (Russo & Silver, 1994). However, slab rollback is only reported for the eastern portion of the Indo-Burma subduction system (Lee et al., 2016). Therefore, we propose that one of the possible explanations for the observed E-W fast orientation from XKS splitting in the Himalayan block is the westward continuation of slab rollback-induced flow along the Burma subduction zone (Liu et al., 2019). The westward absolute plate motion of the Eurasian plate in the hotspot reference frame (Gripp & Gordon, 2002) may also contribute to the E-W anisotropy (Singh et al., 2016), although the slow rate of motion (23 mm/yr) might be too small to produce significant azimuthal anisotropy (Kendall et al., 2022). The upper layer fast orientation of Station H0230 generally aligns with the resulting crustal anisotropy measurements (Figure 5), which could be caused by the lattice-preferred-orientation of crustal anisotropic minerals such as mica due to the northeastward compression between the Indian and Eurasian plates.

4.5. Possible Mantle Upwelling Through a Slab Window

Null measurements are characterized by a lack of XKS energy on the transverse component and can be caused by two situations (Silver & Chan, 1991). The first is that the mantle and crust from the core-mantle boundary to the surface sampled by the XKS ray path are seismically isotropic (“true null”), which also includes the rare scenario when two (or more) layers have mutually orthogonal fast orientations but comparable splitting times (see Liu & Gao, 2013 for a quantitative representation for this situation). The second situation is pseudo null, which occurs when the fast orientation is parallel or orthogonal to the BAZ. For the first situation, null measurements present

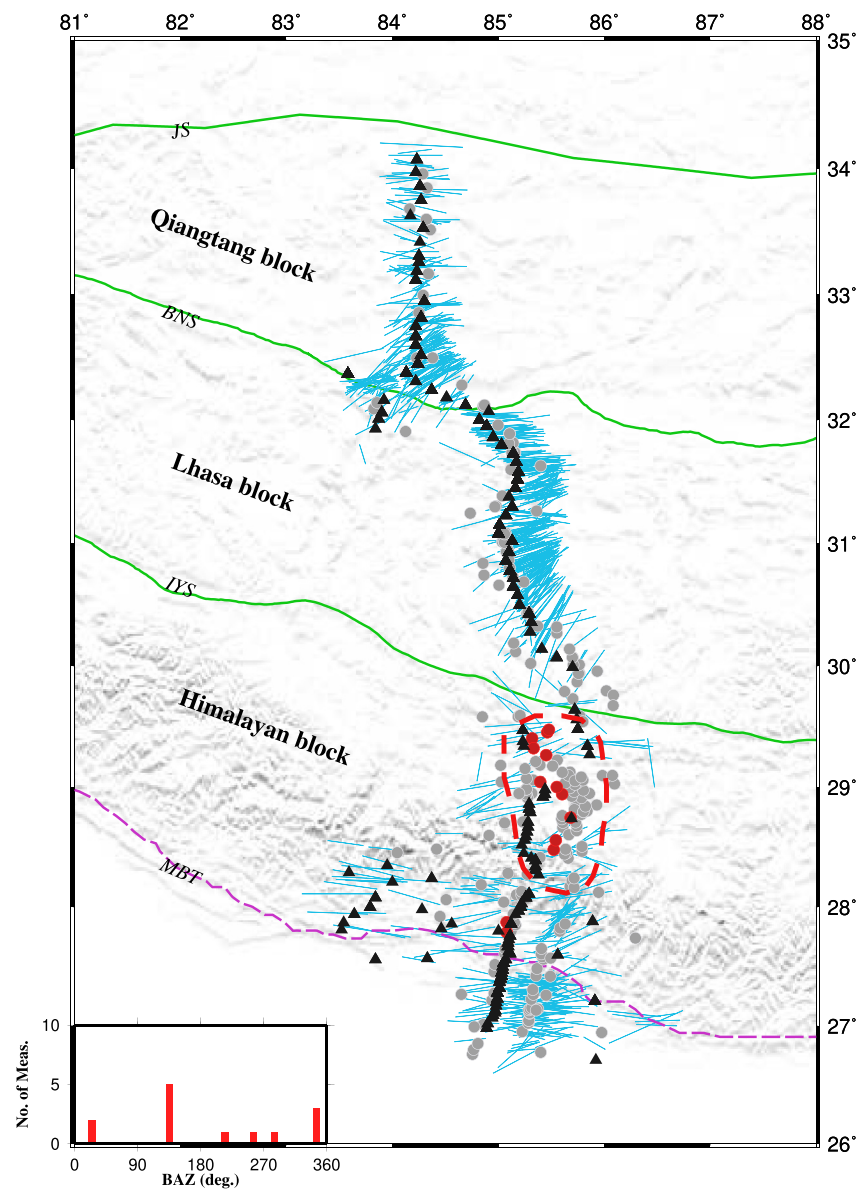


Figure 8. Distribution of individual XKS splitting parameters (blue bars) and true null measurements (red circles) as well as pseudo or unknown null measurements (gray circles) for the study area. Black triangles are seismic stations. Dashed red lines outline an area with a significant clustering of true null measurements. The pie diagrams shown in Figure S8 in Supporting Information S1 indicate the proportion of the XKS phases, and the histogram in the lower left corner displays the number of true null measurements against BAZs.

for events with different BAZs, and for the second situation, null measurements are only from events with similar or orthogonal BAZs. In this study, we apply a three-step procedure to determine true null measurements. First, the coordinates of the ray piercing points of all the null measurements at the estimated anisotropy depth for a given area are calculated. Second, the area is divided into consecutive non-overlapping rectangle bins with a dimension of 0.2° by 0.2° at both the E-W and N-S directions, and the circular average of the BAZs of all the null measurements for each bin is calculated. Third, the BAZs of the individual null measurements in the bin are compared with the average BAZ in the bin to determine if they are true nulls. Specifically, if a null measurement with a difference between the BAZ and the averaged BAZ is greater than 15.0° in the modulo- 90° domain, it is considered a true null (red circles in Figure 8). Admittedly, the resulting spatial distribution of the true null measurements would vary when different bin sizes and threshold values are used. However, testing using different parameters suggests that the area with a concentration of true nulls would not change.

Using the above procedure, an area with concentrated true null measurements in the northern part of the Himalayan block has been identified (Figure 8). For most of the null measurements in this area, the events are from the southeast (lower-left inset in Figure 8). This area is also characterized by an absence of well-defined splitting measurements, which independently confirms the lack of observable azimuthal anisotropy. In this area, seismic tomography studies (Li & Song, 2018; Lü et al., 2024; Nie et al., 2020) imaged a discontinuity in the subducted Indian slab and interpreted it as a slab tear. In addition, geochemical investigations (e.g., Chen et al., 2021) reported anomalously high Sr/Y ratios in adakitic Miocene rocks in the area, and proposed a deep mantle origin, probably from upwelling through a slab tear. On the basis of these observations, we hypothesize that the pervasive true nulls in this area result from mantle upwelling through the slab tear (Figure 7).

5. Conclusions

Joint analyses of SWS and receiver function measurements in the south-central Tibetan plateau reveal systematic variations in crust and mantle seismic anisotropy. The expanded back azimuth coverage, archived through an extended epicentral distance range over previous studies and the inclusion of PKS and SKKS phases in addition to SKS, contribute to a substantial enhancement in the quality and quantity of splitting measurements, especially south of the Indus-Yarlung suture where null measurements were reported by previous studies. Using crustal anisotropy results and optimal anisotropy depth estimates, this comprehensive approach allows better identification and characterization of complex anisotropy patterns. Standard deviation analysis of fast orientations suggests that the source of anisotropy is primarily situated within the mid to lower crust in the Qiangtang block and extends into the upper asthenosphere in both the Himalayan and Lhasa blocks induced by slab subduction and slab rollback along the Burma subduction zone. The clustering of true null measurements near the Bangong-Nujiang suture suggests a significant upwelling of asthenospheric material, likely driven by slab tearing.

Data Availability Statement

All the data used in the study are publicly available from the Seismological Facility for the Advancement of Geoscience Data Management Center, using the BREQ_FAST data requesting procedure. Note that the email-based BREQ_FAST request will be replaced by FetchData and ROVER. The seismic data includes the networks XF (Nabelek, 2002), YL (Sheehan et al., 2001), and Y2 (Roecker & Levin, 2007). The specific data requesting parameters including the cut-off magnitude and epicentral distance range can be found in Section 2. To demonstrate the quality of the measurements, during the review process of this paper, the manually verified XKS results and the crustal anisotropy results from receiver functions can be reviewed at Shen et al. (2024). Figures were made with Generic Mapping Tools versions 4.5.7 and 6.2.0 (Wessel et al., 2019).

Acknowledgments

We thank the Seismological Facility for the Advancement of Geoscience (SAGE) Data Management Center for providing access to the seismic data used in this study. The service for downloading seismic data is funded through the National Science Foundation's Seismological Facility for the SAGE Award under Cooperative Agreement EAR-1724509. Constructive reviews from two anonymous reviewers, the associate editor, and Editor Satoshi Ide are greatly appreciated. The study was partially supported by the U.S. National Science Foundation under awards 1830644 and 2149587 to K.L. and 1919789 to S.G., and the Zhengjiang Provincial Natural Science Foundation of China award No. LR24D060001 to F.K.

References

- Agius, M., & Lebedev, S. (2017). Complex, multilayered azimuthal anisotropy beneath Tibet: Evidence for co-existing channel flow and pure-shear crustal thickening. *Geophysical Journal International*, 210(3), 1823–1844. <https://doi.org/10.1093/gji/ggx266>
- Basuyau, C., Diament, M., Tiberi, C., Hetényi, G., Vergne, J., & Peyrefitte, A. (2013). Joint inversion of teleseismic and GOCE gravity data: Application to the Himalayas. *Geophysical Journal International*, 193(1), 149–160. <https://doi.org/10.1093/gji/ggs110>
- Beaumont, C., Jamieson, R. A., Nguyen, M. H., & Medvedev, S. (2004). Crustal channel flows: 1. Numerical models with applications to the tectonics of the Himalayan-Tibetan orogen. *Journal of Geophysical Research*, 109(B6). <https://doi.org/10.1029/2003jb002809>
- Chen, H., Hou, M., Xiong, F., Tang, H., & Shao, G. (2021). Petrogenesis and geodynamic implications of Miocene felsic magmatic rocks in the Wuyu basin, Southern Gangdese belt, Qinghai-Tibet plateau. *Minerals*, 11(6), 655. <https://doi.org/10.3390/min11060655>
- Chen, W., Martin, M., Tseng, T., Nowack, R., Hung, S., & Huang, B. (2010). Shear-wave birefringence and current configuration of converging lithosphere under Tibet. *Earth and Planetary Science Letters*, 295(1–2), 297–304. <https://doi.org/10.1016/j.epsl.2010.04.017>
- Chen, W. P., & Özalaybey, S. (1998). Correlation between seismic anisotropy and Bouguer gravity anomalies in Tibet and its implications for lithospheric structures. *Geophysical Journal International*, 135(1), 93–101. <https://doi.org/10.1046/j.1365-246x.1998.00611.x>
- Chen, Y., Li, W., Yuan, X., Badal, J., & Teng, J. (2015). Tearing of the Indian lithospheric slab beneath southern Tibet revealed by SKS-wave splitting measurements. *Earth and Planetary Science Letters*, 413, 13–24. <https://doi.org/10.1016/j.epsl.2014.12.041>
- Christensen, N. I. (1984). The magnitude, symmetry and origin of upper mantle anisotropy based on fabric analyses of ultramafic tectonites. *Geophysical Journal International*, 76(1), 89–111. <https://doi.org/10.1111/j.1365-246x.1984.tb05025.x>
- Conrad, C. P., & Behn, M. D. (2010). Constraints on lithosphere net rotation and asthenospheric viscosity from global mantle flow models and seismic anisotropy. *Geochemistry, Geophysics, Geosystems*, 11(5). <https://doi.org/10.1029/2009gc002970>
- Crampin, S. (1981). A review of wave motion in anisotropic and cracked elastic-media. *Wave Motion*, 3(4), 343–391. [https://doi.org/10.1016/0165-2125\(81\)90026-3](https://doi.org/10.1016/0165-2125(81)90026-3)
- Duan, Y., Tian, X., Liang, X., Li, W., Wu, C., Zhou, B., & Iqbal, J. (2017). Subduction of the Indian slab into the mantle transition zone revealed by receiver functions. *Tectonophysics*, 702, 61–69. <https://doi.org/10.1016/j.tecto.2017.02.025>
- Frederiksen, A. W., & Bostock, M. G. (2000). Modelling teleseismic waves in dipping anisotropic structures. *Geophysical Journal International*, 141(2), 401–412. <https://doi.org/10.1046/j.1365-246x.2000.00090.x>

- Fu, Y., Chen, Y., Li, A., Zhou, S., Liang, X., Ye, G., et al. (2008). Indian mantle corner flow at southern Tibet revealed by shear wave splitting measurements. *Geophysical Research Letters*, *35*(2). <https://doi.org/10.1029/2007gl031753>
- Gao, S., & Liu, K. (2009). Significant seismic anisotropy beneath the southern Lhasa Terrane, Tibetan plateau. *Geochemistry, Geophysics, Geosystems*, *10*(2). <https://doi.org/10.1029/2008gc002227>
- Gilligan, A., & Priestley, K. (2018). Lateral variations in the crustal structure of the Indo–Eurasian collision zone. *Geophysical Journal International*, *214*(2), 975–989. <https://doi.org/10.1093/gji/ggy172>
- Gripp, A. E., & Gordon, R. G. (2002). Young tracks of hotspots and current plate velocities. *Geophysical Journal International*, *150*(2), 321–361. <https://doi.org/10.1046/j.1365-246x.2002.01627.x>
- Guo, Z., Gao, X., Yao, H., Li, J., & Wang, W. (2009). Midcrustal low-velocity layer beneath the central Himalaya and southern Tibet revealed by ambient noise array tomography. *Geochemistry, Geophysics, Geosystems*, *10*(5). <https://doi.org/10.1029/2009gc002458>
- Hess, H. H. (1964). Seismic anisotropy of the uppermost mantle under oceans. *Nature*, *203*(4945), 629–631. <https://doi.org/10.1038/203629a0>
- Hirn, A., Jiang, M., Sapin, M., Diaz, J., Nercessian, A., Lu, Q. T., et al. (1995). Seismic anisotropy as an indicator of mantle flow beneath the Himalayas and Tibet. *Nature*, *375*(6532), 571–574. <https://doi.org/10.1038/375571a0>
- Hollister, L. S., & Crawford, M. L. (1986). Melt-enhanced deformation: A major tectonic process. *Geology*, *14*(7), 558. [https://doi.org/10.1130/0091-7613\(1986\)14<558:MDAMTP>2.0.CO;2](https://doi.org/10.1130/0091-7613(1986)14<558:MDAMTP>2.0.CO;2)
- Hsü, K. J., Guitang, P., & Sengör, A. M. C. (1995). Tectonic evolution of the Tibetan plateau: A working hypothesis based on the archipelago model of orogenesis. *International Geology Review*, *37*(6), 473–508. <https://doi.org/10.1080/00206819509465414>
- Hu, N., Li, Y., & Xu, L. (2019). Crustal seismic anisotropy of the Northeastern Tibetan Plateau and the adjacent areas from shear-wave splitting measurements. *Geophysical Journal International*, *220*(3), 1491–1503. <https://doi.org/10.1093/gji/ggz489>
- Huang, W., Ni, J., Tilmann, F., Nelson, D., Guo, J., Zhao, W., et al. (2000). Seismic polarization anisotropy beneath the central Tibetan Plateau. *Journal of Geophysical Research*, *105*(B12), 27979–27989. <https://doi.org/10.1029/2000jb900339>
- Hung, S. H., Chen, W. P., Chiao, L. Y., & Tseng, T. L. (2010). First multi-scale, finite-frequency tomography illuminates 3-D anatomy of the Tibetan Plateau. *Geophysical Research Letters*, *37*(6). <https://doi.org/10.1029/2009gl041875>
- Ismail, W. B., & Mainprice, D. (1998). An olivine fabric database: An overview of upper mantle fabrics and seismic anisotropy. *Tectonophysics*, *296*(1–2), 145–157. [https://doi.org/10.1016/s0040-1951\(98\)00141-3](https://doi.org/10.1016/s0040-1951(98)00141-3)
- Jia, Y., Liu, K. H., Kong, F., Liu, L., & Gao, S. S. (2021). A systematic investigation of piercing-point-dependent seismic azimuthal anisotropy. *Geophysical Journal International*, *227*(3), 1496–1511. <https://doi.org/10.1093/gji/ggab285>
- Jiang, M., Ai, Y., Zhou, S., & Chen, Y. J. (2014). Distribution of the low velocity bulk in the middle-to-lower crust of southern Tibet: Implications for formation of the north–south trending rift zones. *Earthquake Science*, *27*(2), 149–157. <https://doi.org/10.1007/s11589-014-0080-1>
- Jin, Y., McNutt, M. K., & Zhu, Y. S. (1996). Mapping the descent of Indian and Eurasian plates beneath the Tibetan Plateau from gravity anomalies. *Journal of Geophysical Research: Solid Earth*, *101*(B5), 11275–11290. <https://doi.org/10.1029/96jb00531>
- Jolivet, L., Faccenna, C., Becker, T., Tesauro, M., Sternai, P., & Bouilhol, P. (2018). Mantle flow and deforming continents: From India-Asia convergence to pacific subduction. *Tectonics*, *37*(9), 2887–2914. <https://doi.org/10.1029/2018tc005036>
- Kapp, J. L., Harrison, T. M., Kapp, P., Grove, M., Lovera, O. M., & Ding, L. (2005). Nyainqentanglha Shan: A window into the tectonic, thermal, and geochemical evolution of the Lhasa block, southern Tibet. *Journal of Geophysical Research*, *110*(B8). <https://doi.org/10.1029/2004jb003330>
- Kapp, P., Taylor, M., Stockli, D., & Ding, L. (2008). Development of active low-angle normal fault systems during orogenic collapse: Insight from Tibet. *Geology*, *36*(1), 7. <https://doi.org/10.1130/g24054a.1>
- Kendall, E., Faccenda, M., Ferreira, A. M. G., & Chang, S. (2022). On the relationship between oceanic plate speed, tectonic stress, and seismic anisotropy. *Geophysical Research Letters*, *49*(15). <https://doi.org/10.1029/2022gl097795>
- Klemperer, S. L. (2006). Crustal flow in Tibet: Geophysical evidence for the physical state of Tibetan lithosphere, and inferred patterns of active flow. *Geological Society*, *268*(1), 39–70. <https://doi.org/10.1144/gsl.sp.2006.268.01.03>
- Ko, B., & Jung, H. (2015). Crystal preferred orientation of an amphibole experimentally deformed by simple shear. *Nature Communications*, *6*(1), 6586. <https://doi.org/10.1038/ncomms7586>
- Kong, F., Wu, J., Liu, K., & Gao, S. (2016). Crustal anisotropy and ductile flow beneath the eastern Tibetan Plateau and adjacent areas. *Earth and Planetary Science Letters*, *442*, 72–79. <https://doi.org/10.1016/j.epsl.2016.03.003>
- Langille, J. M., Jessup, M. J., Cottle, J. M., Newell, D., & Seward, G. (2010). Kinematic evolution of the Ama Drime detachment: Insights into orogen-parallel extension and exhumation of the Ama Drime Massif, Tibet–Nepal. *Journal of Structural Geology*, *32*(7), 900–919. <https://doi.org/10.1016/j.jsg.2010.04.005>
- Lease, R. O., Burbank, D. W., Zhang, H., Liu, J., & Yuan, D. (2012). Cenozoic shortening budget for the northeastern edge of the Tibetan plateau: Is lower crustal flow necessary? *Tectonics*, *31*(3). <https://doi.org/10.1029/2011tc003066>
- Lee, H., Chung, S., & Yang, H. (2016). Late Cenozoic volcanism in central Myanmar: Geochemical characteristics and geodynamic significance. *Lithos*, *245*, 174–190. <https://doi.org/10.1016/j.lithos.2015.09.018>
- Lei, J., Zhao, D., Xu, X., Xu, Y., & Du, M. (2019). Is there a big mantle wedge under eastern Tibet? *Physics of the Earth and Planetary Interiors*, *292*, 100–113. <https://doi.org/10.1016/j.pepi.2019.04.005>
- Levin, V., & Park, J. (1998). P-SH conversions in layered media with Hexagonally symmetric anisotropy: A Cookbook. *Pure and Applied Geophysics*, *151*(2–4), 669–697. <https://doi.org/10.1007/s000240050136>
- Li, H., Ye, Z., Gao, R., & Huang, X. (2022). A distinct contrast in the lithospheric structure and limited crustal flow across the northeastern Tibetan plateau: Evidence from Vs and Vp/Vs imaging. *Tectonophysics*, *836*, 229413. <https://doi.org/10.1016/j.tecto.2022.229413>
- Li, J., & Song, X. (2018). Tearing of Indian mantle lithosphere from high-resolution seismic images and its implications for lithosphere coupling in southern Tibet. *Proceedings of the National Academy of Sciences*, *115*(33), 8296–8300. <https://doi.org/10.1073/pnas.1717258115>
- Ligorria, J. P., & Ammon, C. J. (1999). Iterative deconvolution and receiver-function estimation. *Bulletin of the Seismological Society of America*, *89*(5), 1395–1400. <https://doi.org/10.1785/bssa0890051395>
- Liu, K., & Gao, S. (2011). Estimation of the depth of anisotropy using spatial coherency of shear-wave splitting parameters. *Bulletin of the Seismological Society of America*, *101*(5), 2153–2161. <https://doi.org/10.1785/0120100258>
- Liu, K., & Gao, S. (2013). Making reliable shear-wave splitting measurements. *Bulletin of the Seismological Society of America*, *103*(5), 2680–2693. <https://doi.org/10.1785/0120120355>
- Liu, L., Gao, S. S., Liu, K. H., Li, S., Tong, S., & Kong, F. (2019). Toroidal mantle flow induced by slab subduction and rollback beneath the Eastern Himalayan syntaxis and adjacent areas. *Geophysical Research Letters*, *46*(20), 11080–11090. <https://doi.org/10.1029/2019gl084961>
- Long, M. D., & Silver, P. G. (2009). Shear wave splitting and mantle anisotropy: Measurements, interpretations, and new directions. *Surveys in Geophysics*, *30*(4–5), 407–461. <https://doi.org/10.1007/s10712-009-9075-1>

- Lü, Z., Lei, J., Kong, Q., Liu, Q., & Sun, J. (2024). Seismic structure of the 2015 Mw7.8 Gorkha earthquake revealed by ambient seismic noise and teleseismic surface wave tomography. *Scientific Reports*, *14*(1), 7921. <https://doi.org/10.1038/s41598-024-57713-8>
- McKenzie, D. (1978). Active tectonics of the Alpine–Himalayan belt: The Aegean Sea and surrounding regions. *Geophysical Journal International*, *55*(1), 217–254. <https://doi.org/10.1111/j.1365-246x.1978.tb04759.x>
- Molnar, P., England, P., & Martinod, J. (1993). Mantle dynamics, uplift of the Tibetan plateau, and the Indian Monsoon. *Reviews of Geophysics*, *31*(4), 357–396. <https://doi.org/10.1029/93rg02030>
- Molnar, P., Fitch, T. J., & Wu, F. T. (1973). Fault plane solutions of shallow earthquakes and contemporary tectonics in Asia. *Earth and Planetary Science Letters*, *19*(2), 101–112. [https://doi.org/10.1016/0012-821x\(73\)90104-0](https://doi.org/10.1016/0012-821x(73)90104-0)
- Nabelek, J. (2002). Collaborative research: Lithospheric scale dynamics of active mountain building along the Himalayan–Tibetan collision zone [Dataset]. *FDSN. International Federation of Digital Seismograph Networks*. https://doi.org/10.7914/SN/XF_2002
- Nabelek, J., Hetenyi, G., Vergne, J., Sapkota, S., Kafle, B., Jiang, M., et al. (2009). Underplating in the Himalaya–Tibet collision zone revealed by the Hi-CLIMB experiment. *Science*, *325*(5946), 1371–1374. <https://doi.org/10.1126/science.1167719>
- Nair, S., Gao, S., Liu, K., & Silver, P. (2006). Southern African crustal evolution and composition: Constraints from receiver function studies. *Journal of Geophysical Research*, *111*(B2). <https://doi.org/10.1029/2005jb003802>
- Nie, S., Tian, X., Liang, X., Chen, Y., & Xu, T. (2020). Pn uppermost mantle tomography of central Tibet: Implication for mechanisms of N–S rifts and conjugate faults. *Tectonophysics*, *788*, 228499. <https://doi.org/10.1016/j.tecto.2020.228499>
- Pang, Y., Zhang, H., Gerya, T. V., Liao, J., Cheng, H., & Shi, Y. (2018). The mechanism and dynamics of N–S rifting in southern Tibet: Insight from 3–D thermomechanical modeling. *Journal of Geophysical Research: Solid Earth*, *123*(1), 859–877. <https://doi.org/10.1002/2017jb014011>
- Pasyanos, M. E., Masters, T. G., Laske, G., & Ma, Z. (2014). LITHO1.0: An updated crust and lithospheric model of the Earth. *Journal of Geophysical Research: Solid Earth*, *119*(3), 2153–2173. <https://doi.org/10.1002/2013jb010626>
- Roecker, S., & Levin, V. (2007). Collaborative research: Imaging the upper mantle beneath the western Tibetan plateau [Dataset]. *FDSN. International Federation of Digital Seismograph Networks*. https://doi.org/10.7914/SN/Y2_2007
- Rümpker, G., Kaviani, A., & Latifi, K. (2014). Ps-splitting analysis for multilayered anisotropic media by azimuthal stacking and layer stripping. *Geophysical Journal International*, *199*(1), 146–163. <https://doi.org/10.1093/gji/eggu154>
- Rümpker, G., & Silver, P. G. (1998). Apparent shear-wave splitting parameters in the presence of vertically varying anisotropy. *Geophysical Journal International*, *135*(3), 790–800. <https://doi.org/10.1046/j.1365-246x.1998.00660.x>
- Russo, R. M., & Silver, P. G. (1994). Trench-parallel flow beneath the Nazca plate from seismic anisotropy. *Science*, *263*(5150), 1105–1111. <https://doi.org/10.1126/science.263.5150.1105>
- Sandvol, E., Ni, J., Kind, R., & Zhao, W. (1997). Seismic anisotropy beneath the southern Himalayas–Tibet collision zone. *Journal of Geophysical Research*, *102*(B8), 17813–17823. <https://doi.org/10.1029/97jb01424>
- Savage, M. K. (1999). Seismic anisotropy and mantle deformation: What have we learned from shear wave splitting? *Reviews of Geophysics*, *37*(1), 65–106. <https://doi.org/10.1029/98rg02075>
- Sheehan, A., Wu, F., & Bilham, R. (2001). Himalayan seismotectonics, Nepal and Tibet [Dataset]. *FDSN. International Federation of Digital Seismograph Networks*. https://doi.org/10.7914/SN/YL_2001
- Shen, C., Gao, S. S., Kong, F., & Kelly, L. H. (2024). Tectonic implications of seismic anisotropy layering beneath the southern Tibetan Plateau revealed by integrated shear wave splitting and receiver function analyses (version 2) [Dataset]. *Figshare*. <https://doi.org/10.6084/m9.figshare.26169310.v1>
- Shi, D., Lü, Q., Xu, W., Yan, J., Zhao, J., Dong, S., & Chang, Y. (2013). Crustal structure beneath the middle–lower Yangtze metallogenic belt in east China: Constraints from passive source seismic experiment on the Mesozoic intra-continental mineralization. *Tectonophysics*, *606*, 48–59. <https://doi.org/10.1016/j.tecto.2013.01.012>
- Silver, P., & Chan, W. (1991). Shear wave splitting and subcontinental mantle deformation. *Journal of Geophysical Research*, *96*(B10), 16429–16454. <https://doi.org/10.1029/91jb00899>
- Silver, P., & Savage, M. (1994). The interpretation of shear-wave splitting parameters in the presence of two anisotropic layers. *Geophysical Journal International*, *119*(3), 949–963. <https://doi.org/10.1111/j.1365-246x.1994.tb04027.x>
- Silver, P. G. (1996). Seismic anisotropy beneath the continents: Probing the depths of geology. *Annual Review of Earth and Planetary Sciences*, *24*(1), 385–432. <https://doi.org/10.1146/annurev.earth.24.1.385>
- Singh, A., Eken, T., Mohanty, D. D., Saikia, D., Singh, C., & Ravi Kumar, M. (2016). Significant seismic anisotropy beneath southern Tibet inferred from splitting of direct S-waves. *Physics of the Earth and Planetary Interiors*, *250*, 1–11. <https://doi.org/10.1016/j.pepi.2015.11.001>
- Singh, A. D., Kumar, M., Raju, P. S., & Ramesh, D. S. (2006). Shear wave anisotropy of the northeast Indian lithosphere. *Geophysical Research Letters*, *33*(16). <https://doi.org/10.1029/2006gl026106>
- Tao, Y., Zhang, H., Zhang, J., Pang, J., Wang, Y., Wu, Y., et al. (2022). Late Cretaceous–Early Cenozoic exhumation across the Yalong thrust belt in eastern Tibet and its implications for outward plateau growth. *Global and Planetary Change*, *216*, 103897. <https://doi.org/10.1016/j.gloplacha.2022.103897>
- Wang, Q., Hawkesworth, C. J., Wyman, D. A., Chung, S., Wu, F. Y., Li, X. H., et al. (2016). Pliocene–Quaternary crustal melting in central and northern Tibet and insights into crustal flow. *Nature Communications*, *7*(1), 11888. <https://doi.org/10.1038/ncomms11888>
- Wessel, P., Luis, J. F., Uieda, L., Scharroo, R., Wobbe, F., Smith, W. H. F., & Tian, D. (2019). The generic mapping Tools version 6 [Software]. *Geochemistry, Geophysics, Geosystems*, *20*(11), 5556–5564. <https://doi.org/10.1029/2019GC008515>
- Wu, C., Tian, X., Xu, T., Liang, X., Chen, Y., Taylor, M., et al. (2019). Deformation of crust and upper mantle in central Tibet caused by the northward subduction and slab tearing of the Indian lithosphere: New evidence based on shear wave splitting measurements. *Earth and Planetary Science Letters*, *514*, 75–83. <https://doi.org/10.1016/j.epsl.2019.02.037>
- Wu, J., Zhang, Z., Kong, F., Yang, B. B., Yu, Y., Liu, K. H., & Gao, S. S. (2015). Complex seismic anisotropy beneath western Tibet and its geodynamic implications. *Earth and Planetary Science Letters*, *413*, 167–175. <https://doi.org/10.1016/j.epsl.2015.01.002>
- Yin, A., & Harrison, T. M. (2000). Geologic evolution of the Himalayan–Tibetan orogen. *Annual Review of Earth and Planetary Sciences*, *28*(1), 211–280. <https://doi.org/10.1146/annurev.earth.28.1.211>
- Zhang, B., Bao, X., Wu, Y., Xu, Y., & Yang, W. (2023). Southern Tibetan rifting since late Miocene enabled by basal shear of the underthrusting Indian lithosphere. *Nature Communications*, *14*(1), 2565. <https://doi.org/10.1038/s41467-023-38296-w>
- Zhang, H., Zhao, D., Yu, C., & Zhao, J. (2016). Varying deformation patterns in central Tibet revealed by radial anisotropy tomography. *Journal of Geophysical Research: Solid Earth*, *121*(5), 3445–3461. <https://doi.org/10.1002/2016jb012832>
- Zhao, W., Nelson, K. D., Che, J., Quo, J., Lu, D., Wu, C., & Liu, X. (1993). Deep seismic reflection evidence for continental underthrusting beneath southern Tibet. *Nature*, *366*(6455), 557–559. <https://doi.org/10.1038/366557a0>
- Zheng, T., Ding, Z., Ning, J., Chang, L., Wang, X., Kong, F., et al. (2018). Crustal azimuthal anisotropy beneath the southeastern Tibetan plateau and its geodynamic implications. *Journal of Geophysical Research: Solid Earth*, *123*(11), 9733–9749. <https://doi.org/10.1029/2018jb015995>

- Zheng, T., Wang, J., Gao, S. S., Ding, Z., Liu, K. H., Yu, Y., et al. (2024). Crustal deformation associated with the Tan-Lu fault zone in east China revealed by receiver function analysis. *Tectonophysics*, *816*, 229014. <https://doi.org/10.2139/ssrn.4598990>
- Zhou, Z., & Lei, J. (2016). Pn anisotropic tomography and mantle dynamics beneath China. *Physics of the Earth and Planetary Interiors*, *257*, 193–204. <https://doi.org/10.1016/j.pepi.2016.06.005>
- Zhu, L., & Kanamori, H. (2000). Moho depth variation in southern California from teleseismic receiver functions. *Journal of Geophysical Research*, *105*(B2), 2969–2980. <https://doi.org/10.1029/1999jb900322>